Chapter 6

6. Strength and Deformability Parameters of the Damaged Zones

6.1 General

The in-situ structure of the rock strata in the zone of influence of a longwall working is disturbed due to the formation of micro and macro fractures and the resulting degradation of their strength and deformability properties. Accurate modelling of the mechanical behaviour of the damaged strata is critical for evaluating the stability of the chain pillar during different stages of its loading. In-situ and laboratory testing do not provide a field representative estimate of the rock mass properties in this zone. They fail to consider strata damage contributed by bedding and lamination planes, rock mass anisotropy, and different scales of the mining-induced fractures.

In this chapter, a systematic approach based on numerical modelling and back-analysis is presented to estimate the strength and deformability properties of the disturbed rock mass above the longwall excavation. Based on the results of previous ground control workers and field measurements in the Indian geo-mining conditions, the extent of zones of disturbance in the overlying strata is identified. The material models for the zones are selected considering the mechanical behavioural aspects of the strata.

The confined uniaxial compression tests on the graded down gob material (Pappas and Mark 1993) were replicated to estimate the model parameters of the Caved zone material and calibrate them using the back-analysis technique. The parameters for modelling Fractured zone and Continuous Deformation zones by using the Ubiquitous joint and the Transversely Isotropic elastic models, respectively, as discussed in Section 3.5, Chapter 3, were estimated

through the back-analysis of the surface subsidence profile. Finally, the modelling results were verified against the findings of already reported work in similar conditions and the field observations in Indian conditions.

6.2 Delimitation of the Zones in the Area of the Excavation

One of the major concerns of the mining engineers and researchers is to find suitable approaches for the evaluation of overlying strata behaviour induced due to the longwall panel extraction. The identification of induced damaged zones and destressed zone above the panel because of longwall extraction is critical for the design of longwall mining. The damaged overlying strata due to the longwall extraction are generally categorised into three zones: Caved zone, Fractured zone, and Continuous Deformation zone (Figure 6.1). The height of destressed zone (HDZ) is considered equivalent to the height up to the Fractured zone above the longwall panel. The effective estimation of the HDZ is crucial during the numerical simulation of the longwall mining because the stresses from this zone are transferred to the adjoining gate roads and chain pillars. HDZ can be estimated based on field observations, previous studies, and the prevailing common theories in similar geological and mining conditions.

Peng (2006), Chekan and Listak (1993) and Turchaninov et al. (1977) reported that the height of the caving zone might vary from 2 to 8 times the extraction height depending on the geological conditions, while Karacan (2010) and Palchik (2002) opined that the caving height ranges from 4 to 11 times the extraction height. Kratzsch (1983) and Karmis et al. (1983) opined that the height of the caving zone could be up to 12 times the extraction height. On the other hand, Singh and Singh (2011), based on field investigations, reported that the caving height could be as high as 15 times the extraction height in Indian geo-mining conditions where the overlying strata are dominated by the presence of massive sandstone rocks. Considering

the outcomes of these previous studies and the field observations reported earlier, the caving height of 15 times the extraction height was considered in this study.

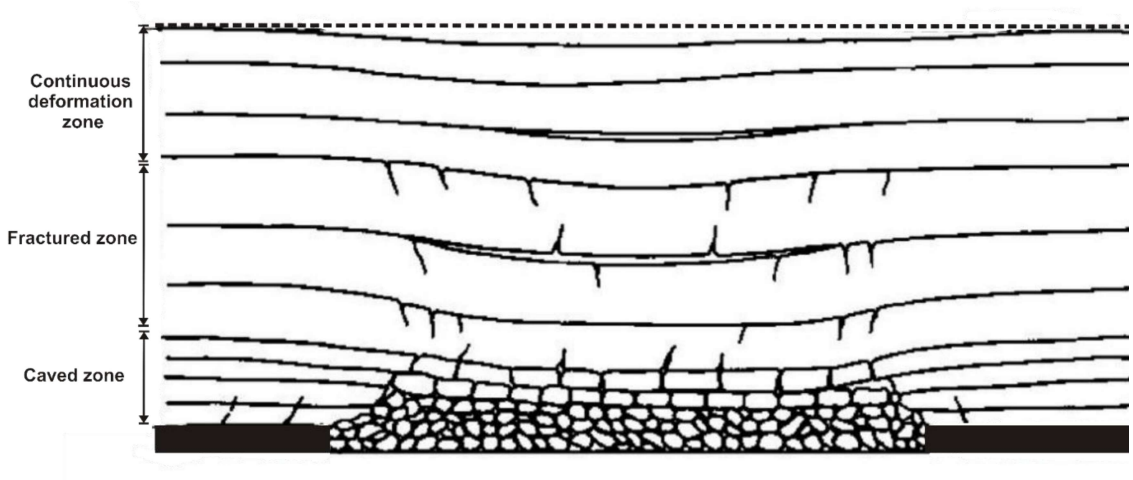

Figure 6.1 The damaged strata above a longwall panel due to extraction of the underlying seam (after Peng and Chiang, 1984)

Rezaei et al. (2015a) investigated the effect of the mining height on the abutment pressure and the Fractured zone thickness. They observed that the thickness of the Fractured zone and the zone of influence of the abutment pressure increased with the extraction height. As per the study conducted by Peng and Chiang (1984), the thickness of the fracture zone can vary between 28 and 42 times the extraction height. Chekan and Listak (1993) and Palchik (1989) suggested that the thickness of the Fractured zone ranges from 20 to 100 times the height of the extraction. Zhang et al. (2011) reported that the height of the Fractured zone varies from 10 to 11 times the extraction height based on the observation of ground subsidence monitored using a borescope in a series of boreholes above a panel of Shangwan Colliery.

Following the above observations and based on initial trial runs of the models, the Fractured zone was modelled above the Caved zone extending up to the surface in case of the shallow depth longwall panels where the depth is less than 100m. The thickness of the Fractured zone was considered as 28 times the extraction height for moderate to high cover depth longwall panels. The abutment angle (the angle subtended by the caving line and the vertical line at the gob edge) of 25° was incorporated in the models in line with typical field observations in Indian coalfields for shallow cover depth workings.

The Continuous Deformation zone spreads between the Fractured zone and the surface. In this zone, the rock mass is damaged due to the disturbance caused by underground excavation, and cracks appear sparsely. The rock mass in this zone behaves elastically. The correct determination of the elastic properties of rock beds within this zone is crucial for the subsidence profile of the model and the distribution of loads at the seam level.

6.3 Selection of Material Models

Proper material model selection is essential for a field representative simulation of mining induced failure and deformation of strata deformation above an excavated area. Hence, a reasonable estimation of load on the surrounding structures around the excavation. The caved goaf undergoes irreversible compaction due to rearrangements of the rock fragments and a decrease in the void ratio under the pressure of the overlying fractured strata. This behaviour of the caved material was modelled using the Double yield model of FLAC^{3D} (Itasca 2015). The model includes a volumetric yield surface, referred to as 'Cap', to consider the permanent volume changes due to isotropic pressure. The hardening behaviour of the cap pressure is activated as a function of volumetric plastic strain following a user-defined piecewise linear

relation. The elastic stiffness evolves as a function of volumetric strain defined in terms of plastic stiffness and the factor (R), which is assumed to be constant.

The failure of the strata in the 'Fractured' zone may occur either by joints, stratification, or rock mass (Alejano et al. 1999). It was assumed that strength features of the joints dominate the mechanical behaviour of the strata due to their highly fractured nature. Hence, the anisotropic yield surface represented by the Ubiquitous-joint model was assigned together with the isotropic elastic model for the deformation of rock mass within this zone. This model includes strength anisotropy due to the plane of weaknesses in the Mohr-Coulomb material model.

The 'Continuous Deformation' zone exhibits elastic anisotropic deformation behaviour before failure (Tajduś 2009, Yao et al. 1993). It was assumed that the deformational aspects of the Continuous Deformation zone primarily represent the mechanical behaviour of the rock mass within this zone. Hence, the Transversely Isotropic model was assigned to the strata in the Continuous Deformation zone. The model considers an independent deformation modulus along the bedding plane and the normal to the bedding plane, and an independent shear modulus.

6.4 Model Parameters for the Caved Goaf Material

The caved goaf material shows strain-hardening characteristics under the combined effect of the sagging overlying fractured stratum and heaving of the floor strata. The compaction process of the gob material has been studied at the laboratory scale by Pappas and Mark (1993). The test results confirmed that the theoretical model proposed by Salamon (1990) could represent the behaviour of the gob material across various rock types. Hence, the parameters of the

Double yield model were determined by comparing the numerical modelling results with Salamon's (1990) results.

Salamon (1990) proposed a hyperbolic stress-strain relationship (Equation 6.1) to define the constitutive behaviour of the goaf material, considering it similar to various other granular media like sand and sundry aggregates. In this equation, $\boldsymbol{\sigma}$ is the stress, $\boldsymbol{E_0}$ is the initial modulus, $\boldsymbol{\varepsilon}$ is the strain and $\boldsymbol{\varepsilon_m}$ is the maximum strain.

$$\boldsymbol{\sigma} = \frac{\mathbf{E_0 \varepsilon}}{\left(\mathbf{1} - \frac{\boldsymbol{\varepsilon}}{\boldsymbol{\varepsilon_m}}\right)} \tag{6.1}$$

The initial modulus $\boldsymbol{E_0}$ was determined using the relation proposed by Yavuz (2004) (Equation 6.2), which was further adjusted by calibrating the model to produce the maximum subsidence as observed in the field, while $\boldsymbol{\epsilon_m}$ was estimated using the initial bulking factor ('b') of the gob material (Equation 6.3).

$$\mathbf{E_0} = \frac{\mathbf{10.39 \sigma_c^{1.042}}}{\mathbf{b^{7.7}}} \tag{6.2}$$

In the above equation, $\boldsymbol{\sigma_c}$ denotes the compressive strength of intact rock fragments.

$$\boldsymbol{\varepsilon_m} = \frac{\mathbf{b - 1}}{\mathbf{b}} \tag{6.3}$$

The initial bulking factor of the goaf material is a function of the extraction height ('h') and the caving height ('h_c') (Equation 6.4). The density of the gob material was estimated using Equation 6.5, considering the principle of conservation of mass.

$$\boldsymbol{b} = \frac{\mathbf{h} + \boldsymbol{h_c}}{\mathbf{h}} \tag{6.4}$$

$$\boldsymbol{\rho_{gob}} = \frac{\boldsymbol{\rho_{imm.}^{avg.}}}{\mathbf{b}} \tag{6.5}$$

where $\boldsymbol{\rho}_{\boldsymbol{imm.}}^{\boldsymbol{avg.}}$ is the thickness weighted average of the density of the immediate roof rocks, and 'b' is the bulking factor of the gob material.

Further, the elastic modulus of the gob material, $\boldsymbol{E_{gob}}$, can be estimated considering that the fragmented gob material can undergo maximum possible compaction to regain its initial elastic moduli following the concept of composite elastic modulus as explained by Harrison and Hudson (2000) (Equation 6.6). In Equation 6.6, 'n' is the number of beds in the caving zone, $\boldsymbol{t_i}$ is the thickness, and $\boldsymbol{E_i}$ is the modulus of elasticity of i^{th} bed.

$$\boldsymbol{E_{gob}} = \frac{\sum_{i=1}^{n} \boldsymbol{t_i}}{\sum_{i=1}^{n} \frac{\boldsymbol{t_i}}{\boldsymbol{E_i}}} \tag{6.6}$$

The Double yield model requires several input parameters to simulate the strain hardening behaviour of the goaf material. The model requires two sets of properties: material and volumetric. The material property comprises elastic constants like bulk and shear modulus, Poisson's ratio, and the Mohr-Coulomb strength parameters such as cohesion, friction angle, tensile strength and dilation angle. The volumetric property includes the ratio (R) of elastic to plastic bulk modulus and the hardening curve defined by the cap pressure table.

The sensitivity analysis carried out by Yadav et al. (2020a) revealed that the bulk and the shear moduli (K and G) are the most critical parameters for Double yield model. The values of K and G should not interfere with the cap pressure table, estimated using the theoretical model up to the expected in-situ vertical stress. The stress-strain characteristics curve remains flattened for the strain values beyond the last entry of the cap pressure table. This understanding can be beneficial for simulating goaf behaviour in supercritical longwall workings where the gob stress becomes constant beyond the cover pressure distance. The last entry in the table was kept commensurate with the expected vertical stress to meet this requirement.

Further, higher values of R were avoided as it limited the elastic strain. The remaining material properties such as cohesion, dilation, friction, and Poisson's ratio did not significantly affect the calibration curve. A constant proportion of the vertical stress to the cap pressure was utilised for the determination of the cap pressure table using the theoretical model for a given set of properties.

A standard approach was employed for calibrating the Double yield model against Salamon's model. It comprised constructing the laboratory scale model, assigning Double yield constitutive material properties, defining initial and boundary conditions, and prescribing a cap pressure table based on the theoretical model in the first step. In the second step, history logs for average vertical stress, cap pressure, total volumetric strain, plastic volumetric strain, and theoretical stress were enabled. In the third step, the model was run for the desired timesteps, and the plots of total volumetric strain vs history records of the other parameters were obtained. Subsequently, the ratio of the in-situ vertical stress to the cap pressure was determined to estimate the cap pressure from the theoretically estimated stress. The plastic volumetric strain was obtained from the total elastic strain in each model. Following these steps, the cap pressure table was formulated, and the model was re-run to obtain the calibrated stress-strain characteristics.

The above approach was verified by experimentally calibrated models for different values of the initial modulus (E_0) and the bulking factor (b). For this, a numerical model was prepared in FLAC^{3D} software to simulate uniaxial compression of gob material, replicating the study of Pappas and Mark (1993), as discussed in Section 3.12, Chapter 3. The value of E_0 varied from 10 to 50 MPa for the value of 'b', ranging between 1.1-1.5. These combinations of E_0 and 'b' represent characteristically different gob material. The model was calibrated for the maximum vertical stress of 25 MPa, corresponding to the cover depth of 1000m. A typical set of properties of the goaf material considered in the Double yield model are summarised in Table 6.1. Figure

6.2 shows the degree of fit of results obtained from the numerical model and the Salamon (1990) model.

Table 6.1 Typical material properties of the Double yield model

Density (kg/m^3)	Bulk Modulus (GPa)	Shear Modulus (GPa)	Dilation angle (°)	Angle of Internal Friction (°)	Multiplier (R)	Poisson's ratio
1800	6	4.28	6	18	5	0.2

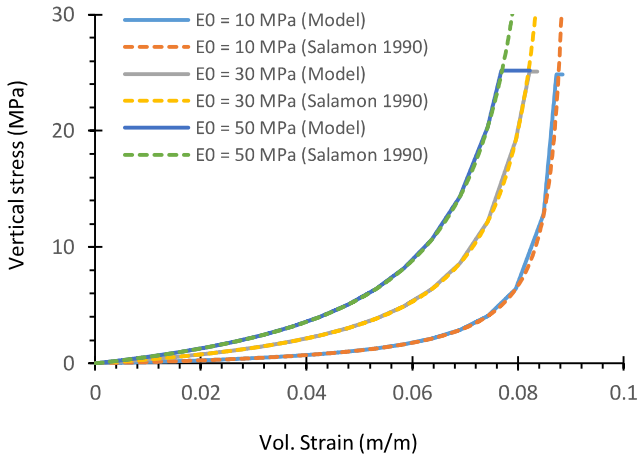

(a) Bulking factor ('b') = 1.1

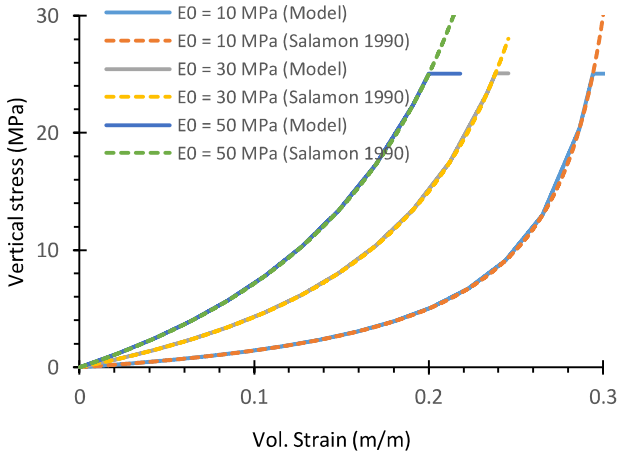

(b) Bulking factor ('b') = 1.5

Figure 6.2 Comparison of the calibrated numerical model results with Salamon (1990) model for varying initial modulus (E_0) and bulking factor ('b')

6.5 Fractured zone Model Parameters

Determining the model parameters of the Fractured zone is a complex process as it involves an increased number of iterations in the back-calculation process to estimate several parameters associated with other zones. However, supercritical longwall panels mined at the shallow depth of cover provide exceptional cases where the Fractured zone spreads up to the surface. Hence, such cases eliminate the Continuous Deformation zone. In this section, four instances of the shallow depth longwall workings were considered to determine the model parameters for the Fractured zone in different geo-mining conditions. A plane strain model along a vertical section parallel to the face at the middle of the panel length was constructed for the study. The model formulation and the modelling scheme are detailed in Section 3.9, Chapter 3.

The supercritical longwall workings considered for this study belong to the Jhanjra Colliery in Raniganj Coalfield, Balrampur and New Kumda mines in Bisharmpur Coalfield, and Rajendra mine in Sohagpur Coalfield. For convenience, these workings are cited as 'A', 'B', 'C', and 'D', respectively, in this thesis. Table 6.2 shows the basic geo-mining parameters of these case studies.

Table 6.2 The geo-mining details of the supercritical longwall panels

Working	Mine	Coal seam	Panel	Face length (m)	Depth from surface (m)	Extraction height (m)
'A'	Jhanjra	RVII	W2	120	60.5	3.7
'B'	Balrampur	Passang	P1	150	50.1	2.4
'C'	New Kumda	Passang	K5	150	71	2.2
'D'	Rajendra	Burhar VIB	P2	150	74	2.2

The characteristics and geotechnical properties of the roof layers for these workings are given in Table 6.3.

Table 6.3 Characteristics of the roof strata and their geotechnical properties in the supercritical workings

Strata	Rock type	Thickness (m)	RQD (%)	Density (kg/m^3)	σ_c (MPa)	σ_t (MPa)	Young's Modulus (GPa)
Working 'A'							
Overburden	Shaly sst, coal, shale, Fg-mgsst, weathered rock	49.96	50	2261	34.03	2.70	6.43
Main roof	Fgsst, intercalation	5.67	63	2261	34	3	6.43
Immediate roof	Mgsst, sandy shale	4.57	79	2256	28.53	2.47	8.73
Coal seam	Coal	4	40	1394	30.00	3.00	2
Working 'B'							
Overburden	Weathered rock	20	40	1789	11.58	1.25	3.29
Main roof	Cgsst to mgsst, very cgsst, Mgsst	24.6	71	2021	15.11	1.86	4.66
Immediate roof	Mgsst with shale lamination	5.5	40	2024	11.00	1.50	3.00
Coal seam	Coal	2.4	40	1400	23.80	2.50	2.00
Working 'C'							
Overburden	Sandstone, shale, weathered rock	28.53	41	1789	16.39	0.85	5.08
Main roof	Sandstone, shale	24.20	59	2021	20.52	1.26	6.07
Immediate roof	Sandstone, shale	18.27	58	2024	19.98	1.07	6.08
Coal seam	Coal	2.2	40	1400	18.04	1.81	2.00
Working 'D'							
Overburden	Sandstone, weathered rock	29.00	40	1957	8.17	0.82	1.66
Main roof	Sandstone	18.00	53	2175	24.55	2.45	6.55

Immediate roof	Sandstone	27.00	54	2098	18.72	1.87	4.57
Coal seam	Coal	3.00	40	1400	20.58	1.96	2.00

The general formulation of numerical models and the simulation schemes for estimating the Ubiquitous joint parameters are described in Section 3.9, Chapter 3. Table 6.4 shows the basic input to the numerical model of the four workings.

Table 6.4 Rock mass input properties of Workings 'A', 'B', 'C', and 'D'

	Thickness (m)	**Density kg/m^3**	**Shear Mod. (GPa)**	**Bulk Mod. (GPa)**	**Tensile strength (MPa)**	**Cohesion (MPa)**
Working 'A'						
Overburden	49.96	2261	2.57	4.29	0.67	1.99
Main Roof	5.67	2261	2.57	4.29	0.85	2.51
Immediate Roof	4.57	2256	3.49	5.82	0.98	2.63
Coal	4	1394	0.80	1.33	0.60	1.91
Floor	50	2300	2.57	4.29	0.67	1.99
Working 'B'						
Overburden	20.00	1789	1.32	2.19	0.25	0.54
Main Roof	24.60	2021	1.86	3.10	0.66	1.25
Immediate Roof	5.50	2024	1.20	2.00	0.30	0.51
Coal	2.4	1400	0.80	1.33	0.50	1.52
Floor	50	2300	1.86	3.10	0.66	1.25
Working 'C'						
Overburden	28.53	1789	2.03	3.38	0.17	0.78
Main Roof	24.20	2021	2.43	4.05	0.37	1.41
Immediate Roof	18.27	2024	2.43	4.05	0.31	1.34
Coal	2.2	1400	0.80	1.33	0.36	1.15
Floor	50	2300	2.43	4.05	0.37	1.41
Working 'D'						
Overburden	29.00	1957	0.66	1.11	0.16	0.38
Main Roof	18.00	2175	2.62	4.37	0.65	1.52
Immediate Roof	27.00	2098	1.83	3.05	0.50	1.17
Coal	3.00	1400	0.80	1.33	0.39	1.31
Floor	50.00	2300	2.62	4.37	0.65	1.52

As previously mentioned, the rock mass strength of the coal seam and strata were estimated using the approach suggested by Singh and Singh (2009). The initial estimates of the joint properties were referred to from the works of previous researchers. Sainsbury and Sainsbury (2017) used joint cohesion ($\boldsymbol{c_j}$) of 100 kPa and joint friction angle ($\boldsymbol{\phi_j}$) of $\mathbf{27°}$ to study the behaviour of sedimentary rock mass with naturally occurring random and orthogonal cross joints with various joint spacing. Alejano et al. (1999) estimated the joint strength parameters for the rock mass in the Fractured zone using the laboratory test results and the Mohr-Coulomb strength criterion, considering the scale effect and the surface subsidence profile in various geo-mining conditions. The estimated average value of joint cohesion, $\boldsymbol{c_j}$ was 125 kPa and joint friction, $\boldsymbol{\phi_j}$ was $\mathbf{27°}$. The joint tension limit ($\boldsymbol{\sigma_j^t}$) was considered to be zero in these studies.

In the initial trial runs, it was observed that the maximum surface subsidence increased with the decreasing joint strength parameters and vice-versa, while it decreased with an increase in the initial modulus of the goaf material and vice-versa. Based on the initial trial runs, it was found that the joint strength parameters reported by Alejano et al. (1999) were suitable for the considered supercritical workings for calibrating the model subsidence with the subsidence profile obtained from Saxena (2003) subsidence model. The initial tangent modulus, $\boldsymbol{E_0}$, for the calibrated models to match the maximum subsidence at the surface were found to be varying from 4.2 - 8 MPa (Figure 6.3). Figure 6.4 compares the subsidence profile obtained from the numerical model and the Saxena (2003) model. The model observed profile is in good agreement with the expected profile.

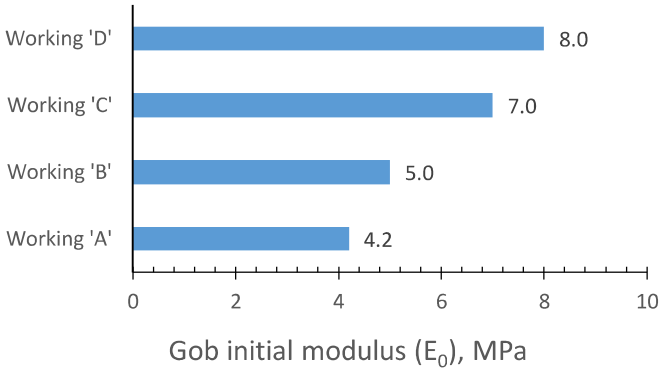

Figure 6.3 Bar chart illustrating the values of initial gob modulus in the four supercritical workings

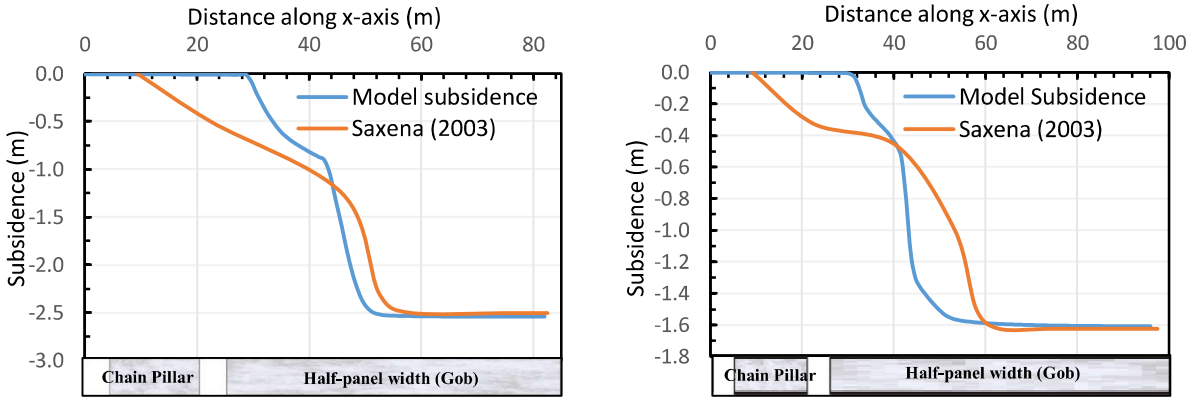

Mine 'A'

Mine 'B'

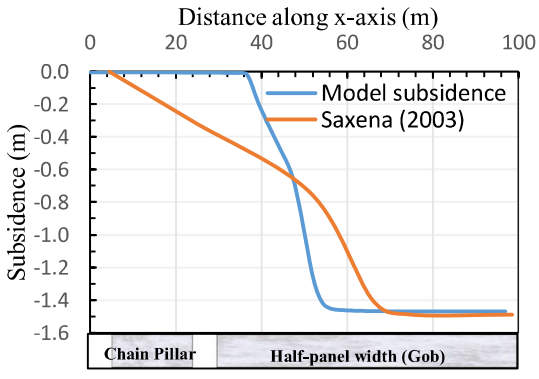

Mine 'C'

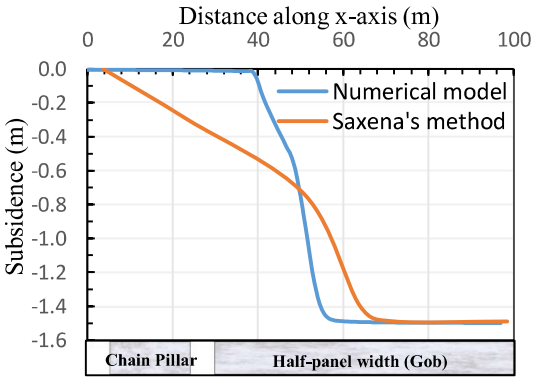

Mine 'D'

Figure 6.4 Comparison of model subsidence results with the empirical subsidence model (Saxena, 2003)

The generally observed subsidence profile in most cases reported worldwide is continuous, where the extent of subsidence at the surface extends beyond the excavation area following the angle of draw. The four workings presented above belong to unique geo-mining conditions where the panel width to depth ratio is greater than two, and the Fractured zone extends up to the surface. Such conditions lead to a stepped subsidence profile at the surface, as confirmed by previous studies reported in Singh and Yadav (1995).

6.6 Model Parameters for the Continuous Deformation zone

After determining the parameters of the Fractured zone, the next step was to develop an approach for the evaluation of model parameters for the 'Continuous Deformation zone (CDZ)'. After several experimental studies, the 'transversely isotropic' model was selected for modelling CDZ, as adopted by Goldstein (1966), Alejano et al. (1999), and Tajduś (2009). In this model, the plane of isotropy (say local axes '1' and '2') is considered, where the elastic properties in the plane are independent of that along the normal to the plane (say local axis '3'). The plane of isotropy is defined by the dip direction (dd) and the dip angle (dip) of the plane. Young's modulus ($\mathbf{E_1 = E_2}$) and Poisson's ratio ($\boldsymbol{\nu_{12} = \nu_{21}}$) are required as input parameters to define the elastic properties in the plane, whereas shear modulus ($\mathbf{G_{13}}$) along with Young's modulus ($\mathbf{E_3}$) and Poisson's ratio ($\boldsymbol{\nu_{13}}$) are required to characterise the elastic behaviour in any plane normal to the isotropy plane.

Four subcritical longwall panels at moderate to high cover depth were considered from different geo-mining conditions to determine the parameters of their Continuous Deformation zone using the transversely isotropic model. These workings belong to JK 5, PVK 5, VK 7, and Adriyala Longwall Projects (ALP) in Godavari Valley Coalfields. For convenience, these workings are referred as 'P', 'Q', 'R', and 'S', respectively. Table 6.5 shows the basic geo-

mining parameters of these case studies. The characteristics and the average geotechnical properties of the roof layers for these workings are shown in Table 6.6. The general formulation of the numerical model and its simulation scheme is described in Section 3.9, Chapter 3. Table 6.7 shows the input data of the rock mass properties used in the numerical model of workings.

Table 6.5 The geo-mining details of the subcritical longwall panels

Working	Mine	Coal seam	Panel	Face length (m)	Depth (m)	Extraction height (m)
'P'	JK5	Queen	3	135	203	3.0
'Q'	PVK5	I	21	150	212	3.0
'R'	VK7	I	4	150	188	2.7
'S'	ALP	I	1	250	465	3.5

Table 6.6 The characteristics of the roof strata and their associated geotechnical properties in the considered subcritical workings

Strata	Rock type	Thickness (m)	RQD (%)	Density (kg/m^3)	σ_c (MPa)	σ_t (MPa)	Young's Modulus (GPa)
Working 'P'							
Overburden	Grey Sandstone, shale	156.70	80	2229	25.30	2.58	7.84
Main roof	Fg-cgsst, Shale, coal, carb. shale	30.80	78	2227	25.73	2.64	7.84
Immediate roof	Shale, coal, shaly coal	6.82	50	2218	33.46	3.83	9.74
Coal seam	Coal	15.68	47	1914	26.90	3.01	2.00
Working 'Q'							
Overburden		166.34	76	2050	12.46	1.07	3.86
Main roof	Cgsst, carb. clay	15.94	66	2050	12.46	1.07	3.86
Immediate roof	Cgsst, carb. clay	30.02	80	2045	10.02	0.97	3.01
Coal seam	Coal	3	40	1400	23.16	1.54	2.00
Working 'R'							
Overburden	Sandstone, shale, clay etc.	159.68	67	2061	11.21	2.02	3.11
Main roof 2	Grey sandstone, shale	15.85	82	2078	11.50	2.17	3.56
Main roof 1	Grey sandstone, shale	12.35	69	2080	11.60	2.17	3.59

Immediate roof	Coal	8.52	40	1440	18.04	1.80	2.00
Coal seam	Coal	2.70	40	1440	18.04	1.80	2.00
Working 'S'							
Overburden	Cgsst	410.00	50	2046	16.77	1.96	5.20
Main roof	Mgsst, Cg-vcgsst, Cgsst, shalycoal	29.40	84	1964	13.22	1.25	2.86
Immediate roof	Cg-vcgsst, Mgsst	23.20	89	2030	13.86	1.07	4.28
Coal roof	Coal, shalycoal	2.40	43	1870	27.58	2.30	2.00
Coal seam	Coal	3.50	40	1400	27.58	2.30	2.00

Table 6.7 Rock mass properties of Workings 'P', 'Q', 'R', and 'S'

	Thickness (m)	**Density kg/m^3**	**Shear Mod. (GPa)**	**Bulk Mod. (GPa)**	**Tensile strength (MPa)**	**Cohesion (MPa)**
Working 'P'						
Overburden	156.70	2229	3.14	5.23	1.03	2.36
Main Roof	30.80	2227	3.14	5.23	1.04	2.36
Immediate Roof	6.82	2218	3.89	6.49	0.95	2.66
Coal Roof	5.68					
Coal	3.00	1914	0.80	1.33	0.70	2.01
Coal Floor	7.00					
Floor	43.00	2300	3.14	5.23	1.03	2.36
Working 'Q'						
Overburden	166.34	2050	1.55	2.58	0.41	1.11
Main Roof	15.94	2050	1.55	2.58	0.35	0.96
Immediate Roof	30.02	2045	1.20	2.00	0.39	0.94
Coal	3.00	1400	0.80	1.33	0.31	1.48
Floor	50.00	2300	1.55	2.58	0.35	0.96
Working 'R'						
Overburden	159.68	2061	1.25	2.08	0.68	0.87
Main Roof2	15.85	2078	1.42	2.37	0.89	1.10
Main Roof1	12.35	2080	1.44	2.39	0.75	0.94
Immediate Roof	8.52	1440	0.80	1.33	0.36	1.15
Coal	2.7	1440	0.80	1.33	0.36	1.15
Floor	50	2300	1.42	2.37	0.89	1.10
Working 'S'						
Overburden	395.00	2046	2.80	4.67	0.49	0.98
Main Roof	29.40	1976	1.14	1.91	0.52	1.29
Immediate Roof	23.20	2026	1.71	2.85	0.49	1.96
Coal Roof	2.40	1592	0.80	1.33	0.47	1.80
Coal	3.50	1592	0.80	1.33	0.47	1.80
Floor	100	2046	2.08	3.47	0.49	0.98

The magnitude of the subsidence and the shape of the subsidence profile is significantly dependent on the elastic and shear moduli of the rock mass in the Continuous Deformation zone, which are difficult to estimate (Alejano et al., 1999). In the present study, these elastic parameters of the transversely isotropic model were evaluated in two steps. In the first step, their initial values were roughly estimated based on the findings of previous studies and simple relationships. In the second step, the values of the parameters were finalised based on a numerical benchmarking procedure.

The elastic modulus of the rock mass can be estimated from the compressive strength of the intact rock and the Geological Strength Index (GSI), using Equation 6.7 (Hoek et al. 2002)

$$E = \left(1 - \frac{D}{2}\right)\sqrt{\frac{\sigma_{ci}}{100}}\,10^{((GSI-10)/40)}\ \text{GPa} \tag{6.7}$$

for $\sigma_{ci} < 100$ MPa

where σ_{ci} is the intact rock compressive strength in MPa, D is the degree of disturbance to the rock mass, and GSI is the Geological Strength Index, the value of which is estimated based on the block size and surface conditions of the joints. Cai et al. (2007) opined that when the rock mass is subjected to disturbance, the block size of the rock mass lowers to the 'disintegrated' category, and the joint surface conditions move towards the 'poor' category in the GSI nomogram (Figure 6.5).

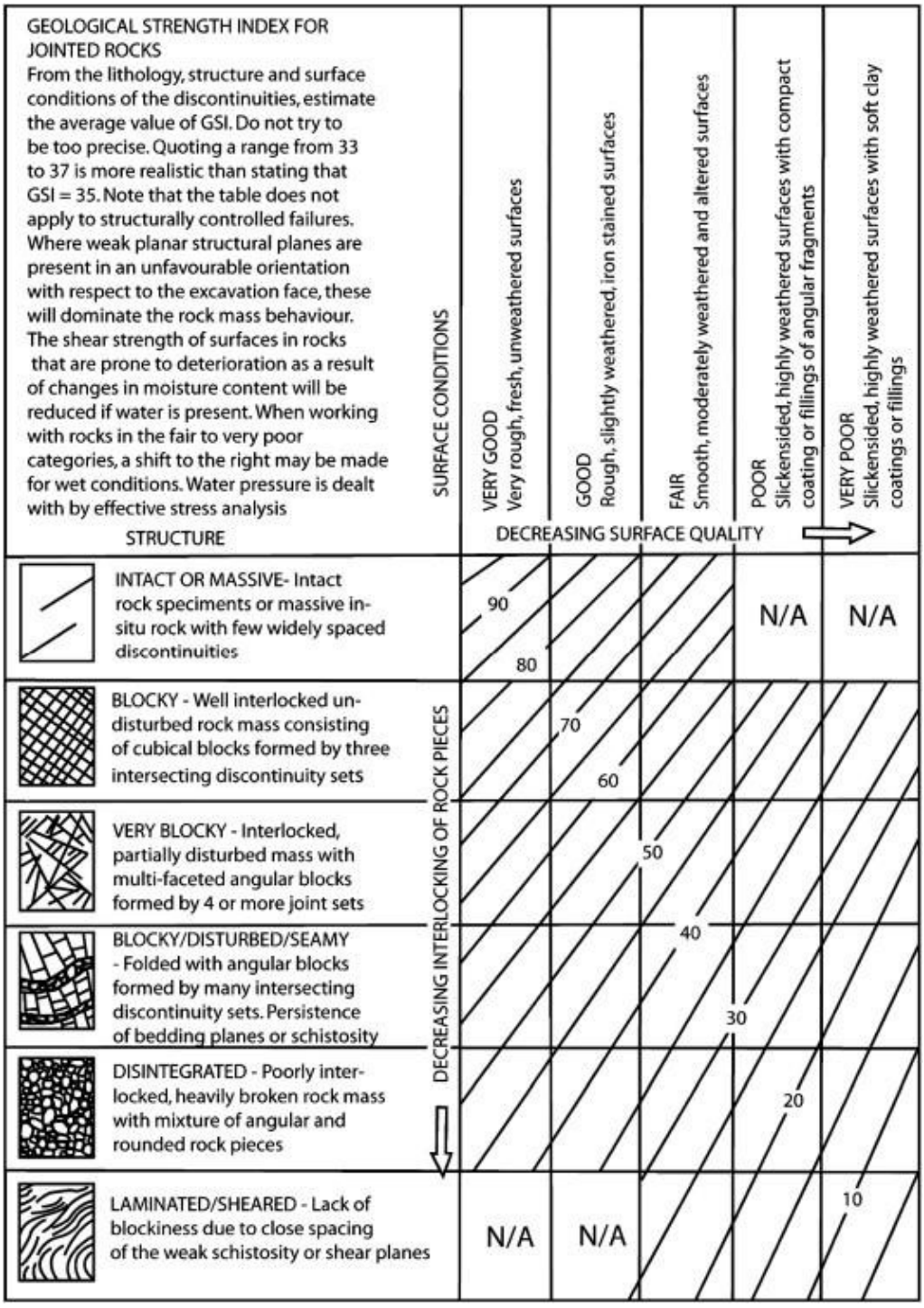

Figure 6.5 Geological Strength Index chart (after Marinos and Hoek, 2000)

Tajduś (2009) used GSI ranging from 28 to 40 for the rock mass in the 'CDZ' to model the surface subsidence profile. The ratio between $\mathbf{E_3}$ and $\mathbf{E_1}$ was assumed to be 1.78 by Yao et al. (1993) and 1.72 by Alejano et al. (1999) in a similar analysis (local axes '1' and '2' represent the horizontal plane and axis '3' represent the plane normal to it). Tajdus (2009) found this ratio as 6.67 based on the back analysis of the measured subsidence. Singh (1973) suggested that the shear modulus, $\mathbf{G_{13}}$, should be $\mathbf{E_3/20}$, whereas Alejano et al. (1999) estimated the value of $\mathbf{G_{13}}$ as 33MPa based on the back-analysis. Tajdus (2009) used the value of $\mathbf{G_{13}}$ ranging from 11 to 23MPa for various rock types in the numerical model of the Continuous Deformation zone.

The preliminary modelling results showed that the magnitude and shape of the subsidence profile were significantly dependent on the ratio between $\mathbf{E_3}$ and $\mathbf{E_1}$ and $\mathbf{G_{13}}$. The magnitude of maximum subsidence increased with the increasing ratio, whereas the subsidence slope above the panel edge was not significantly correlated with the ratio. On the other hand, the magnitude of the maximum subsidence along with the subsidence slope increased substantially with decreasing value of $\mathbf{G_{13}}$ while the maximum subsidence increased with the decreasing initial modulus ($\boldsymbol{E_0}$) of the goaf material.

Based on the above observations, along with the parallel iterative modelling, the ratio between $\mathbf{E_3}$ and $\mathbf{E_1}$ and the value of $\mathbf{G_{13}}$ reported by Alejano et al. (1999) were found to be suitable to calibrate the model observed subsidence against the subsidence obtained from Saxena's (2003) model for the given subcritical workings. The final values of the parameters associated with the transversely isotropic model were estimated as GSI = 30, the ratio of $\mathbf{E_3}$ and $\mathbf{E_1}$ = 1.72 and $\mathbf{G_{13}}$=33MPa. The initial modulus, $\boldsymbol{E_0}$, for the calibrated models were found to be varying from 5 to 76 MPa for the workings under study (Figure 6.6). The comparative plot (Figure 6.7) of the model observed subsidence profile concerning the Saxena (2003) estimates and the field observations show an excellent agreement.

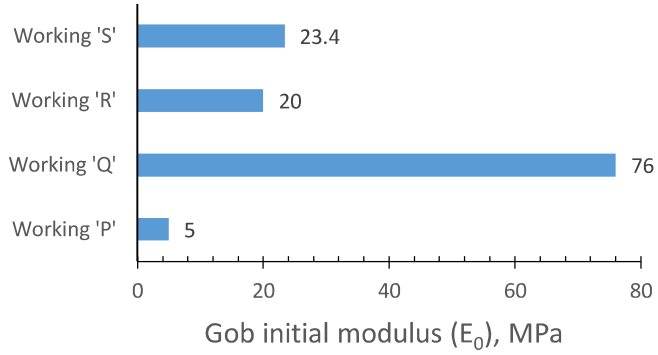

Figure 6.6 Bar chart illustrating the values of initial gob modulus in the four subcritical workings

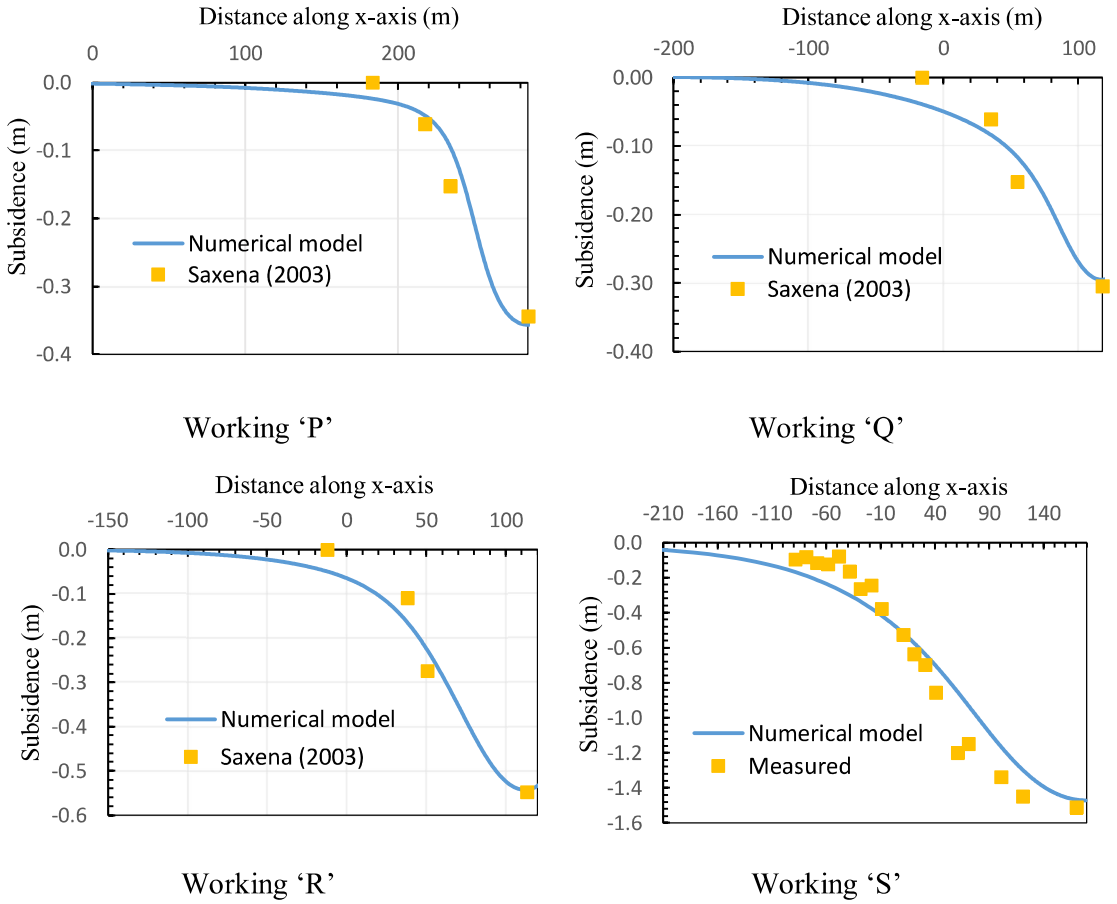

Figure 6.7 Comparison of modelled subsidence results with the empirical model (Saxena, 2003) and in the case of Working 'S' with field measured subsidence

6.7 Verification of Modelling Results

The subsidence calibrated models were verified in terms of the side abutment load, decay profile of abutment stress, and the goaf stress recovery. Figures 6.8 (a) and (b) show the distribution of the In-situ and the Induced vertical stress for supercritical Working 'A' and subcritical Working 'P', respectively. The respective figures for the rest of the workings are attached in Annexure V. It is seen that the vertical stress is uniformly distributed prior to mining. After mining, the stress from the soft goaf material is transferred over the side abutment, including the chain pillar and solid coal block. The redistribution of stress leads to stress relaxation in the gob and concentration along the abutment.

The side abutment stress has a peak value of 2.68 and 2.83 times the in-situ vertical stress for Working 'A' and Working 'P', respectively. This vertical stress decreases from its peak stress to the in-situ stress level at a distance of 75 m in the former and 140 m in the case of the latter from the panel edge, called 'Load Transfer Distance' (LTD). The decay profile of the side abutment stress is in close agreement with the profile proposed by Wilson (1983). The Wilson (1983) decay profile showed a tight fit with the model observed decay profile for the side abutment load of 20 MN/m and 206 MN/m for Working 'A' and Working 'P', respectively.

On the other hand, the stress in the caved goaf rose non-linearly from the goaf edge to attain the maximum stress recovery of almost 100% at 0.33H (20 m) distance, called 'Cover Pressure Distance' (CPD) in the case of supercritical Working 'A'. The maximum pressure recovery (MPR) of almost 68% was realised at the distance of 0.32H (64 m) in the case of Working 'P'. Stress distribution patterns similar to the Working 'A' were also observed for the remaining supercritical Workings 'B', 'C' and 'D' and similar to the Working 'P' were observed for the rest of the subcritical Workings 'Q', 'R', and 'S', as shown in Appendix II.

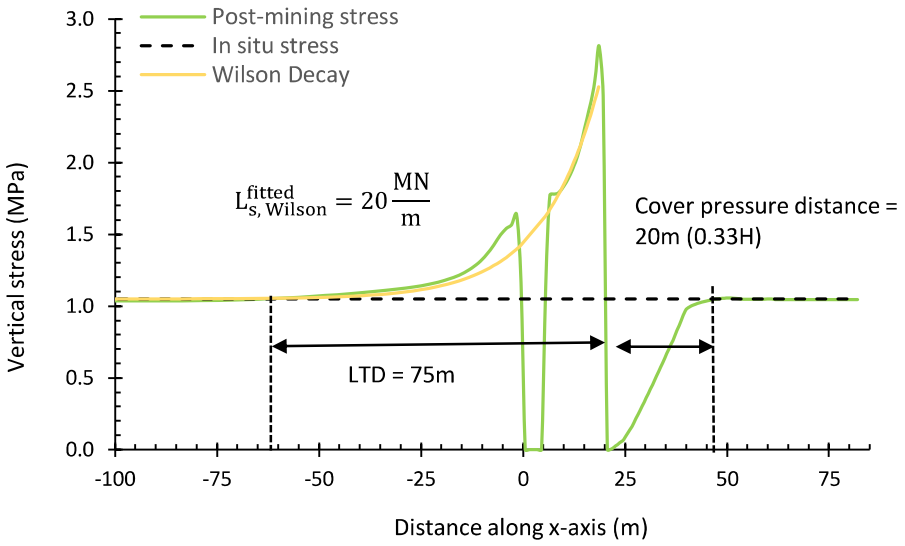

(a)

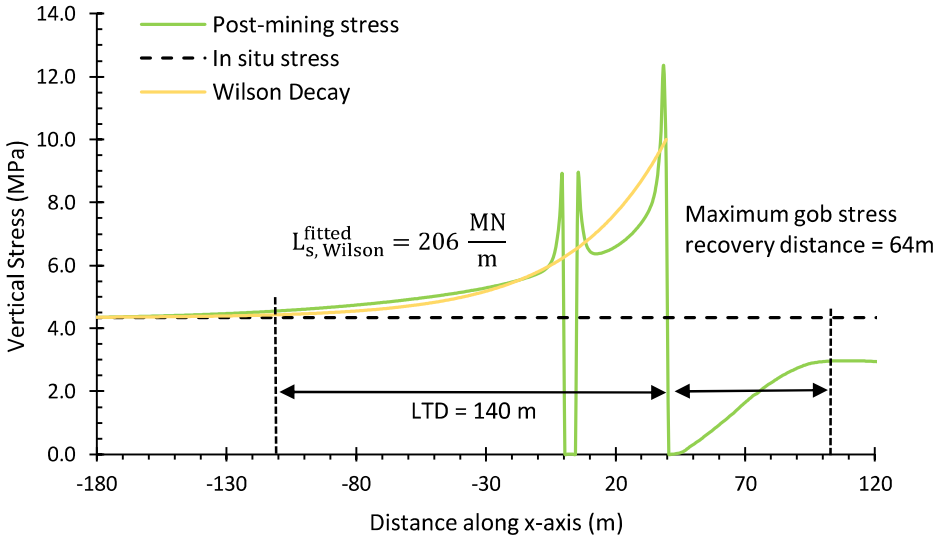

(b)

Figure 6.8 Distribution of vertical stress at the seam level at the pre-mining stage (black dotted line), post-mining stage (solid green line), and Wilson's (1983) abutment stress decay curve fitted to the model abutment stress profile (solid yellow line) for (a) Working 'A' and (b)Working 'P'. The contour at the bottom of the chart depicts vertical stress distribution at the seam level.

Figure 6.9 summarises the modelling results of the four supercritical and four subcritical workings in terms of side abutment load, the maximum pressure distance (MPD), peak side abutment stress, and LTD. The model observed side abutment load corroborated sufficiently with Mark (1987) (Figure 6.9 (a)). The maximum pressure recovery in the four supercritical workings was equal to cover pressure. The CPD in the goaves of the supercritical workings varied from 0.33H to 0.48H. In contrast, MPD in the goaves of subcritical workings varied from 0.12H to 0.32H, which is in close agreement with the field observed CPD that varied between 0.12H to 0.6H (Smart and Haley, 1987; Wilson, 1981; King and Whittaker, 1971; Choi and McCain, 1980; Mark, 1987; and Sheorey, 1993) (Figure 6.9 (b)). The peak abutment stress for the workings varied between 2.00 and 3.42 times the in-situ vertical stress, which is in line with the peak abutment stress observed in different workings in Indian geo-mining conditions as reported in Singh and Singh (2009), Behera et al. (2020b) and Yadav et al. (2020a) (Figure 6.9 (c)). The maximum goaf pressure recovery was 54 – 79% in the supercritical workings.

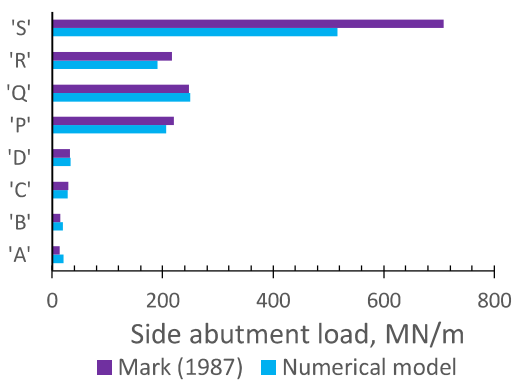

(a)

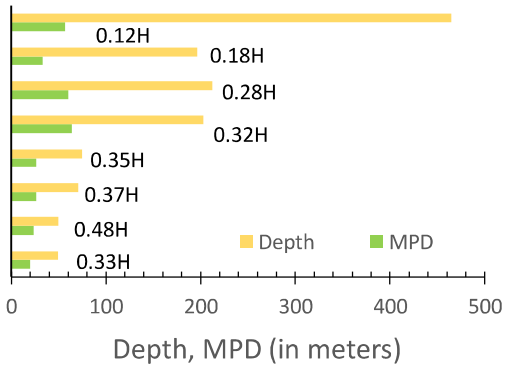

(b)

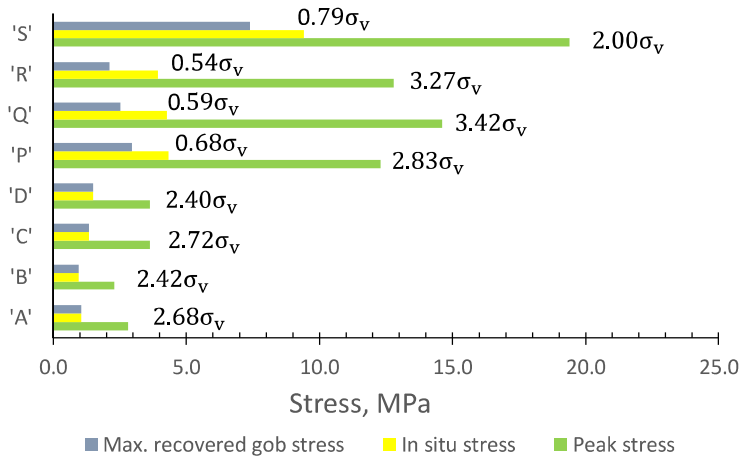

(c)

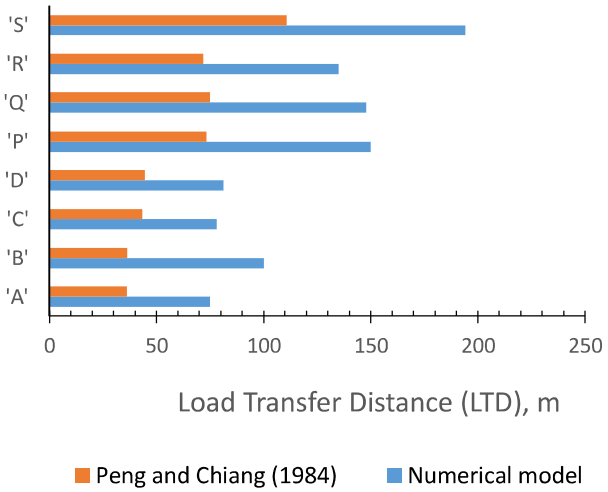

(d)

Figure 6.9 Bar charts illustrating (a) the side abutment load and its comparison with Mark (1987), (b) maximum pressure distance (MPD), (c) peak side abutment stress and maximum recovered gob stress, and (d) load transfer distance (LTD) and its comparison with Peng and Chiang (1984) in the supercritical and subcritical workings

The ratio between the model observed LTD and the value estimated using Peng and Chiang (1984) formula varied between 1.8 and 2.7 (Figure 6.9 (d)). Larson et al. (2015) reported that the LTD could be significantly higher than the estimates of Peng and Chiang (1984), depending upon the geological and mechanical properties of the overlying strata. Singh et al. (2011) observed that the zone of influence is the function of the cavability and the cover depth. Given the strong and massive nature of the rock beds, the model findings are also in line with these observations.

6.8 Summary

This chapter discussed the constitutive models and the approach for estimating the constitutive model parameters of Caved, Fractured and Continuous Deformation zones in longwall workings and their validation using numerical modelling. The heights of the caved and the Fractured zones were estimated using the findings of previous studies and field measurements in Indian geo-mining conditions. The goaf material in the Caved zone was modelled using the Double yield model, while the Fractured zone was simulated using the Ubiquitous-joint model. The transversely isotropic model was assigned the Continuous Deformation zone.

The confined uniaxial compression test on the graded down goaf material, as reported by Pappas and Mark (1993), was replicated to estimate the model parameters of the goaf material using the back-analysis technique. A standard method was developed to estimate the site-specific parameters of the goaf material. The approach was also verified for experimental calibration models representing characteristically different gob material (Figure 6.2).

Based on the back-analysis of the surface subsidence profile using the hit-and-trial technique, the suitable strength and deformability parameters of the Ubiquitous-joint and transversely isotropic models were determined. During the back-analysis, the initial modulus of the goaf

material was adjusted until the maximum subsidence in the model matched the expected value. For estimating the strength parameters of the embedded joints in the Ubiquitous-joint model, the models of four supercritical shallow depth workings were studied, where the Fractured zone extended up to the surface. In the second stage, the deformability parameters of the transversely isotropic model were estimated for four subcritical longwall workings at moderate to high depth of cover. The parameters of the transversely isotropic model and the initial goaf modulus were adjusted to calibrate the model for expected subsidence while deriving the parameters of the Ubiquitous joint model for these working using the understanding developed in stage 1. The joint strength parameters of the Ubiquitous-joint model and the ratio between $\mathbf{E_3}$ and $\mathbf{E_1}$ and the value of $\mathbf{G_{13}}$ of the 'Transversely isotropic' model reported by Alejano et al. (1999) were found to be suitable to calibrate the model observed subsidence with the field observations and that obtained from the Saxena (2003) model.

The initial modulus of goaf varied from 4.2-76 MPa in the calibrated models. The cohesion and friction angle of the rock joints in the Fractured zone was 125 kPa and 27°, respectively. The average Geological Strength Index (GSI) to determine the rock mass modulus from laboratory modulus was 30. The ratio of modulus in the horizontal direction (E_1) to that in the vertical direction (E_3) was estimated as 1.72. The shear modulus in the vertical direction (G_{33}) was determined as 33MPa. The outcome showed that the rock mass had significantly reduced deformation properties in this zone.

The stepped and discontinuous subsidence profiles were observed in shallow depth supercritical, while continuous subsidence profile was observed in the moderate to high depth subcritical workings. The outcomes of the subsidence calibrated models were verified using the findings of previous studies and field observations in Indian geo-mining conditions. The stress in the goaf recovered to the cover pressure at a distance of 0.35 to 0.48H for the four

supercritical workings. In contrast, it recovered to 54-79% of the cover pressure distance of 0.12H – 0.32H in the subcritical workings.

The decay profiles of the side abutment stress were in good agreement with the exponential decay law proposed by Wilson (1983). The model observed side abutment load corroborated sufficiently with the estimates of Mark (1987). The peak abutment stress varied from 2.26 to 3.42 times the in-situ vertical stress, which is in close agreement with the typical observations in the Indian coalfields. However, the model observed load transfer distance (LTD) was significantly greater (1.8-2.7 times) than that calculated using Peng and Chiang (1984), owing to the strong and massive nature of superincumbent strata in Indian conditions. The overall finding was in line with Singh et al. (2011) and Larson (2015).